Preprints (www.preprints.org) | NOT PEER-REVIEWED | Posted: 28 September 2016 doi:10.20944/preprints201609.0113.v1

Article

Microphytobenthos Primary Production Estimated by Hyperspectral Reflectance

Vona Méléder [1,*], Johann Lavaud [2,3], Alexandre Barnett [2], Bruno Jesus [1] and Laurent Barillé [1]

[1] Mer Molécules Santé (MMS) – EA 21 60, Université de Nantes, BP 92208, Nantes Cedex 44322, France; Bruno.Jesus@univ-nantes.fr (B.J.); laurent.barille@univ-nantes.fr (L.B.)
[2] Littoral Environnement et Sociétés (LIENSs) – UMR 7266, CNRS/Université de La Rochelle, Institut du Littoral et de l'Environnement, 2 rue Olympe de Gouges, La Rochelle 17000, France; Johann.Lavaud@takuvik.ulaval.ca (J.L.); barnettalexandre@gmail.com (A.B.)
[3] Takuvik– UMI 3376, CNRS/Université Laval, Département de Biologie, Pavillon Alexandre Vachon, 1045 avenue de la Médecine, Québec, QC G1V 0A6, Canada
* Correspondence: vona.meleder@univ-nantes.fr; Tel.: +33-(0)2-51-12-56-56

Abstract: Monitoring photosynthesis is a great challenge to improve our knowledge of plant productivity at the ecosystem level, which may be achieved using remote-sensing techniques with synoptic abilities. The main objective of the current study is to take up this challenge for microphytobenthos (MPB) primary production in intertidal mudflats. This was achieved by coupling hyperspectral radiometry (reflectance, ρ and second derivative, δδ) and PAM-fluorometry (non-sequential light curve, NSLC) measurements. The later allowed the estimation of the primary production via the light use efficiency (LUE) and the electron transport rate (ETR) whereas ρ allowed to estimate pigment composition and optical absorption cross-section (a*). Five MPB species representative of the main growth forms: epipelic (benthic motile), epipsammic (benthic motile and non motile) and thycoplanktonic (temporarily resuspended in the water column) were lighted at increasing light intensity from dark to 1950 µmol photons.m^{-2}.s^{-1}. After spectral measurements, a* was retrieved using a radiative transfer model and several radiometric indices were tested for their capacity to predict LUE and ETR. The spectral estimation of these two photosynthetic variables was subsequently compared to the values estimated by PAM-fluorometry. Results showed that different responses related to the xanthophyll cycle (de-epoxydation state) were observed for the three growth-forms with increasing light levels. However, a single relationship with radiometric index was not affected by species/growth-forms, i.e. $\delta\delta_{496/508}$, called the MPB_{LUE} index to predict LUE and ETR. This index has the potential to be applied to air borne hyperspectral imagery for large-scale assessment of MPB production.

Keywords: microphytobenthos; intertidal mudflat; primary production; hyperspectral; growth forms; LUE; ETR

1. Introduction

Microphytobenthos (MPB) assemblages are composed of photosynthetic bacteria and microalgae that colonize benthic sediments. Typically, diatoms are the dominant group forming golden-brown biofilms at the sediment surface during low tides [1–3]. Exhibiting very high primary productivity rates that can result in contributions of up to 50% of the total estuarine autochtonous primary production [4], these biofilms provide essential ecosystem services (e.g. food sources for various trophic webs, sediment stabilization via exopolysaccharide secretion (EPS) cohesion, mediation of nutrients fluxes).

However, MPB spatial and temporal variability is a constraint for large-scale assessment and the estimation of its contribution at the ecosystem level is then limited. Most techniques used to assess MPB primary production rates, require single point *in situ* measurements which are often inadequate to capture the spatial variability at the ecosystem level (for a review see [5]). Synoptic informations have been obtained by time-consuming extensive field sampling campaigns [6], or of remote sensing approaches are increasingly used to describe MBP.

Currently, remote sensing studies have mainly focused on quantifying MPB biomass [7–12] and no algorithm exists yet to estimate MPB primary production from remote sensing imagery. However, monitoring photosynthesis from Space, has been recently proposed for land resources (for a review see [13]). It is a great challenge to improve our knowledge of the main drivers and resources constraints of plant productivity and it is needed for predicting impacts of climate change [8,13] and management of costal ecosystems [7,11]. The main objective of the current study is to take up this challenge for MPB primary production.

This was achieved by coupling PAM-fluorometry measurements for estimating primary production [14–16], and spectroradiometry of five MPB species representative of the main growth forms. Growth-forms are known to strongly affect eco-physiological response to light exposure: Non Photochemical Quenching (NPQ) and xanthophyll cycle (XC) patterns [17,18]. Epipelic (moving freely between sediment particle) and epipsammic species (living in close association with individual sand grain) show respectively low and high NPQ values and XC efficiency during high light exposure, whereas thycoplanktonic species show a light response similar to epipelon [17]. Because of these different eco-physiological responses features, different radiometric indices are expected to estimate primary production for the different growth forms (i.e. epipelon/thycoplankton*vs*, epipsammon). We propose here the first spectral index based on MPB growth forms spectral properties to estimate primary production via the ETR (electron transport rate) that could be applied to airborne and satellite hyperspectral images and offers promising prospects for global primary productivity assessment of intertidal MPB biofilms.

2. Materials and methods

2.1. Diatoms culturing

Five diatoms species were selected from a previous study [17] to carry out spectroradiometric and PAM-fluorescence measurements. These species were isolated from natural MPB biofilms and are kept in the Nantes Culture Collection (NCC WDCM 856) (Figure 1). *Navicula phyllepta* (CCY 9804) and *Entomoneis paludosa* (NCC 18.1) are epipelic motile species; *Biremis lucens* (NCC 360.2) and *Planothidium delicatulum* (NCC 363) are epipsammic respectively motile and non-motile species; and

Preprints (www.preprints.org) | NOT PEER-REVIEWED | Posted: 28 September 2016 doi:10.20944/preprints201609.0113.v1

Plagiogrammopsis vanheurckii (NCC 186.2) is a thycoplanktonic species. All diatoms were grown in batch cultures at 20°C in sterile artificial F/2 medium [19], at 20 µmol photon.m^{-2}.s^{-1} and a 16h:8h light:dark photoperiod. Cultures were acclimated during 2 weeks before experiments. Diatom suspensions were diluted to a final concentration of 10 mg Chl*a*.L^{-1} before each experiment. For further details, see [17].

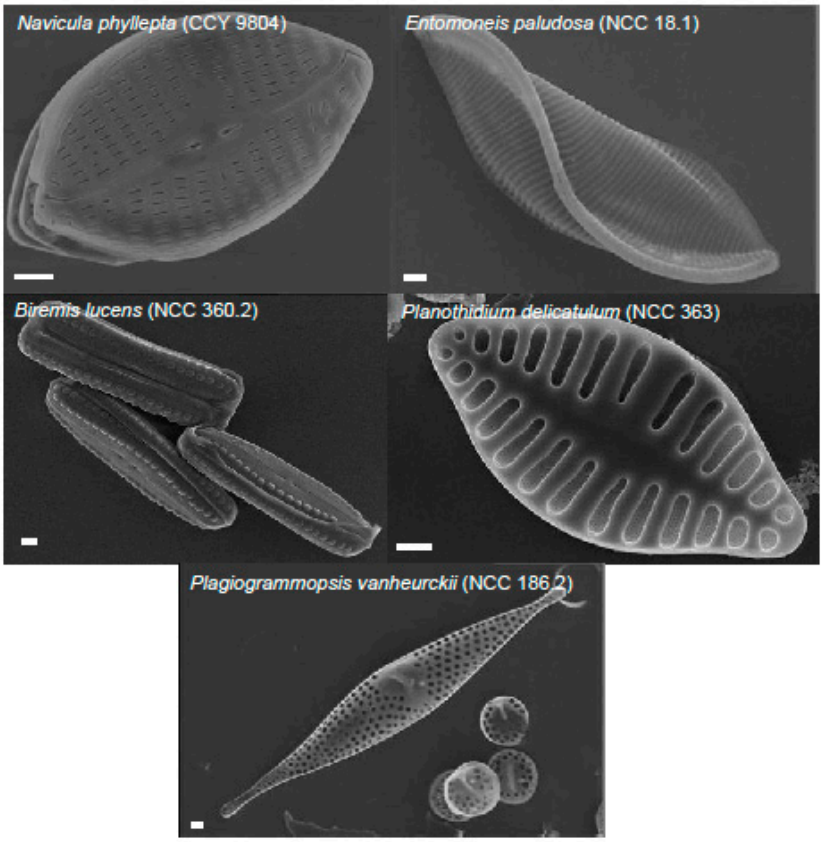

Figure 1. Specimens of the five diatom species viewed in scanning electron microscopy. Scale bars represent 1 µm. Credits Nantes Culture Collection (NCC). *Navicula phyllepta* and *Entomoneis paludosa* belong to the epipelic growth form; *Biremis lucens* and *Planothidium delicatulum* belong to the epipsammic one; *Plagiogrammopsis vanheurckii* is thycoplanktonic.

Preprints (www.preprints.org) | NOT PEER-REVIEWED | Posted: 28 September 2016 doi:10.20944/preprints201609.0113.v1

2.2. Light use efficiency (LUE) and relative electron transport rate (rETR) estimation by PAM fluorometry

PAM fluorescence measurements were performed with a Diving-PAM fluorometer (Walz, Effeltrich, Germany) on a 2.5 ml stirred and 20°C controlled diatom suspension [20]. Minimum fluorescence yield (F_o), maximum fluorescence yield (Fm) and maximum PSII quantum yield (Fv/Fm) were was measured after 15 min dark-adaptation with a saturating pulse of 3600 µmol photons.m^{-2}.s^{-1} (duration 0.4 ms). This was followed by non-sequential light curve (NSLC) measurements [21] using continuous light (KL-2500 lamp, Schott, Mainz, Germany) applied for 5 min at 9 light intensities (E) (48–1950 µmol photons.m^{-2}.s^{-1}). A saturating pulse was applied to the end of each light level to measure the minimum fluorescence yield in light adapted state (F') and the maximum fluorescence yield in light acclimated state (F_m'). PSII effective quantum yield (Φ PS II), non-photochemical quenching (NPQ) and relative electron transport rate (rETR) were calculated with equation 1, 2 and 3, respectively. According to [14], the Φ PS II can also be considered as the light utilization efficiency (LUE).

$$NPQ = (F_m/F_m')-1 \quad \text{eq. 1}$$

$$\Phi \text{ PS II} = LUE = (Fm'-F')/Fm' \quad \text{eq. 2}$$

$$rETR = LUE \times E \quad \text{eq. 3}$$

 doi:10.20944/preprints201609.0113.v1

2.3. Spectroradiometry

At the end of each PAM measurement a volume of 0.5 mL diatom suspension was sampled, immediately diluted in 5 mL of artificial seawater and deposited on anisopore™ polycarbonate membrane filter (Isopore™1.2 µm, 25 mm RTTP filters, Merck Millipore, Darmstadt, Germany) by slow filtration limiting degradation of cells [22,23]. This 5 mL volume allowed to homogenously cover membrane filters with a ~ 13 mg Chl a.m^{-2} layer, a representative biomass value encountered at the mudflat surface [10]. This value remains below saturation threshold occurring for values greater than 40 mg Chl*a*.m^{-2} [10]. All spectral measurements were performed immediately after filtration on wet membrane filters deposited over a black background. This precaution allowed to avoid multiple background reflectance which could trigger the xanthophyll cycle if the background is highly reflected as observed in pre-experimentation using *Navicula phyllepta* (Figure S1). Five measurements per membrane filter were performed using an ASD FieldSpec3 spectrometer (300–2500 nm, sampling: 1 nm, spectral resolution: 4–10 nm, property of the Laboratory of Planetology and Geodynamic (LPG-UMR 6112 of the University of Nantes) to determine radiance (mW.cm^{-2}.nm^{-2}.sr^{-1}). The light source was provided by an internal halogen lamp (300-2500 nm) and the distance between the membrane filter and the ASD optical fiber was kept constant by using the ASD High Intensity Contact Probe. This procedure minimizes errors associated with stray light. Reflectance (ρ, dimensionless) was calculated as the ratio between the radiance of the cells on membrane filters and the incident radiance measured on a perfect diffuser (Spectralon® 99%). Reflectance was standardized (ρ_{std}) to reflectance value at 925 nm, known to be invariable with diatom biomass to facilitate comparisons between spectra

[23,24]. Reflectance of a wet membrane filter with 5 mL of artificial seawater was measured at the beginning of each series of measurement and used as a control.

Second derivative of reflectance spectra ($\delta\delta$) were calculated following [15] and second derivative peaks were assigned to pigment absorption properties according to [24]. To facilitate the comparison between spectra, the second derivative values were standardized ($\delta\delta_{std}$) to the maximum value between 620 and 640 ($\delta\delta_{Chl\ c}$), corresponding to Chl *c* maximum red absorption.

Several radiometric indices were calculated with the objective of estimating LUE and rETR by radiometry. These indices were calculated using *in vivo* second derivative spectra absorption features and absorption properties previously published [15,25–27]. For a first set of indices, the biomass effect was removed by using Chl *c* absorption band ($\delta\delta_{Chl\ c}$) as suggested by [15]. However, because Chl *c* amount could vary between species for a similar light environment and could lead to ratio variations due to species and not to light condition, a second set of indices were constructed using only pigments absorption band involved in the xanthophyll cycle: the diadinoxanthin (DD) and its de-epoxydized form, the diatoxanthin (DT).

Each index was tested to predict LUE. Predicted values of LUE were compared to measured one by PAM-fluorometry (eq. 2) for a new data set, using linear regression (see Data processing and model validation). The most efficient index was selected and used to calculate rETR (eq 3). To calculate the absolute ETR, optical cross-section values, a* (m^2.mg Chl a^{-1}) were retrieved from reflectance spectra using the radiative transfer model MPBOM (MicroPhytoBenthos Optical Model, [22]) as proposed by [24]:

$$ETR = rETR \times a^* \qquad \text{eq. 4}$$

Preprints (www.preprints.org) | NOT PEER-REVIEWED | Posted: 28 September 2016 doi:10.20944/preprints201609.0113.v1

With a* corresponding to the average optical cross-section in the red domain between 670 and 685 nm Chl *a* absorption (=Qy band) [24,28,29].

2.4. Pigment analyses by High Liquid Chromatography (HPLC)

After each PAM and radiometry measurement, 1mL was filtered (Isopore^{TM}1.2 µm, 25 mm RTTP filters, Merck Millipore, Darmstadt,Germany) and immediately frozen in liquid nitrogen for pigment analysis. Pigments were extracted in a cold mixture (4°C) of 90%methanol/0.2 M ammonium acetate (90/10 vol/vol) and 10% ethyl acetate. Injection, HPLC device (Hitachi Lachrom Elite, Tokyo, Japan), pigment identification and quantification [30] is detailed in [17]. All pigments were normalized to Chl *a* content (g.g Chl a^{-1}). Xanthophyll de-epoxidation state was calculated following eq. 5.

$$DES = (DT-DT_0)/(DD+(DT-DT_0)\times 100 \quad \text{eq. 5}$$

where DD is the epoxidized diadinoxanthin, DT is the de-epoxidized diatoxanthin after 5 min light exposure and DT_0, the amount of DT before light exposure. DES calculated this way takes into account the de-epoxidation of DD into DT that specifically occurs during the 5 min light exposure of the NSLC.

2.5. Data processing and model validation

The construction of model to predict LUE and ETR by radiometric indices was achieved using measurements performed on culture replicate of *Navicula phyllepta* and *Biremis lucens*, respectively an epipelic and an epipsammic growth form. Model significance was tested by linear regression (R software) and only radiometric indices explaining more than 40 % (R^2>0.4) of LUE variability measured by PAM fluorometry were selected.

 doi:10.20944/preprints201609.0113.v1

Validation of these selected models was carried out by comparing LUE measured by PAM-fluorometry with LUE predicted by radiometric indices for an independent data set from *Entomoneis paludosa*, *Planothidium delicatulum* and *Plagiogrammopsis vanheurckii* cultures, respectively an epipelic, an epipsammic and a thycoplanktonic growth form. Models with the lesser root mean square error (RSME) were thus used for further calculation of ETR (eq. 4).

3. Results

3.1. Xanthophyll cycle pigments

All diatom main pigments (Table 1), Chl *c*, fucoxanthin (Fuco), β-caroten and the pool of xanthophyll (DD+DT) showed stable pigment to Chl *a* ratios during exposures, but varied with species (2 way ANOVA: $p>0.2$ for light exposure; $p<0.001$ for species). The only pigment ratio that changed with light intensities was the xanthophyll cycle DES ratio estimating the conversion of the DD into DT with increasing light intensity (Figure 2). As expected (see [17]), the epipelic growth form showed the lowest DES values (reaching 17.37% ± 2.26 SD) together with thycoplankton (reaching 20.72 % ± 0.76 SD). Epipsammic growth form showed the highest value (reaching 32.6 % ± 4.65 SD). The stability in the pool of xanthophyll pigments (DD+DT) indicated that no DT was synthesized '*de novo*' during illumination, but were only arose from the de-epoxydation of the DD due to the activation of the xanthophyll cycle.

Preprints (www.preprints.org) | NOT PEER-REVIEWED | Posted: 28 September 2016 doi:10.20944/preprints201609.0113.v1

Table 1. Relative content of pigment expressed in $g.g^{-1}$ Chl *a* of each strain used. Values are the mean of ratios obtained at the end of each exposure (from 0 to 1950 µmol $photon.m^{-2}.s^{-1}$) ± variation coefficient. Growth form is notified for each strain. Mean values varied with species ($p<0.001$), but not with light exposure ($p>0.05$).

	Chl *c*	Fuco	β car	DD+DT
Navicula phyllepta (epileplic)	15.41 ± 0.03	58.93 ± 0.01	3.78 ± 0.04	7.58 ± 0.06
Biremis lucens (epipsammic non-motile)	15.26 ± 0.02	56.80 ± 0.02	1.14 ± 0.22	9.68 ± 0.08
Entomoneis paludosa (epipelic)	18.91 ± 0.01	73.52 ± 0.01	3.59 ± 0.06	6.74 ± 0.04
Planothidium delicatulum (epipsammic motile)	17.57 ± 0.09	59.59 ± 0.09	1.25 ± 0.14	9.37 ± 0.10
Plagiogrammopsis vanheurckii (tychoplanktonic)	27.18 ± 0.05	92.78 ± 0.07	1.27 ± 0.2	9.95 ± 0.21

Preprints (www.preprints.org) | NOT PEER-REVIEWED | Posted: 28 September 2016 doi:10.20944/preprints201609.0113.v1

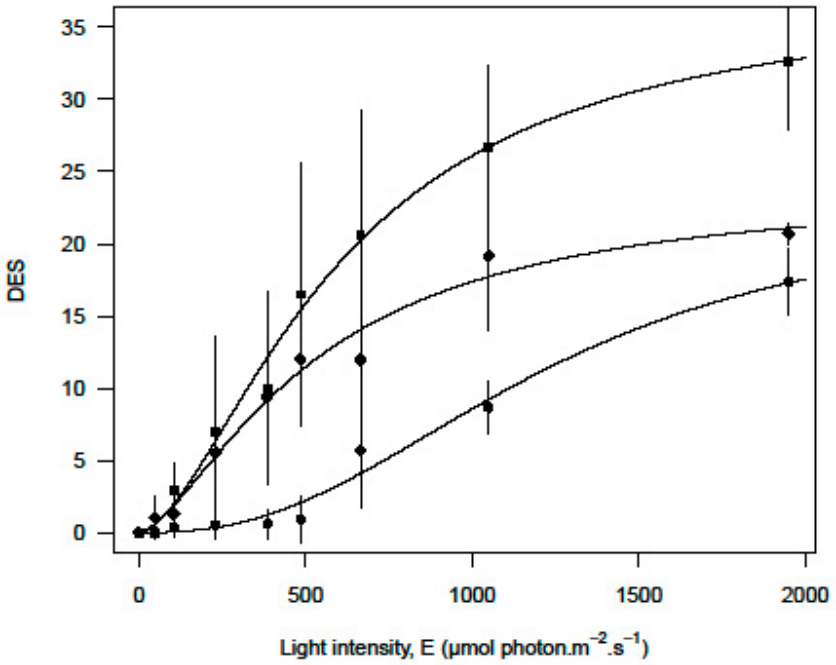

Figure 2. DES *versus* light intensity after 5 min exposure for the three growth forms: ●Epipelic (*Navicula phyllepta* and *Entomoneis paludosa*); ■Epipsammic (*Biremis lucens* and *Planothidium delicatulum*); ◆Thycoplanktonic (*Plagiogrammopsis vanheurckii*). Averaged DES were fitted using the model proposed by [31], vertical bars represent standard deviation.

3.2. Light use efficiency estimation based on PAM fluorescence

LUE and NPQ measured by PAM-fluorometry changed inversely with E: while NPQ increased, LUE decreased with increasing E. Consequently, LUE and NPQ showed inversed relationships with DES (Figure 3) and both could be predicted using DES (eq.6 and eq.7):

Preprints (www.preprints.org) | NOT PEER-REVIEWED | Posted: 28 September 2016 doi:10.20944/preprints201609.0113.v1

$NPQ = 1^{E}10^{-3} \times (DES)^2 + 26.3^{E}10^{-3} \times (DES) + 45.8^{E}10^{-3}$ ($R^2 = 0.94$, $p<0.001$) eq. 6

$LUE = 0.2^{E}10^{-3} \times (DES)^2 - 11.9^{E}10^{-3} \times (DES) + 679^{E}10^{-3}$ ($R^2 = 0.78$, $p<0.001$) eq. 7

Maximum NPQ values were reached by *B. lucens* (more than 2.0) for the highest light intensity corresponding to the highest DES (Figure 3a). LUE lowest values (≤ 0.5) were mainly observed in the two epipsammic species (*B. lucens* and *P. delicatulum*), even if *N. phyllepta* also showed low LUE at high light intensities (Figure 3b).

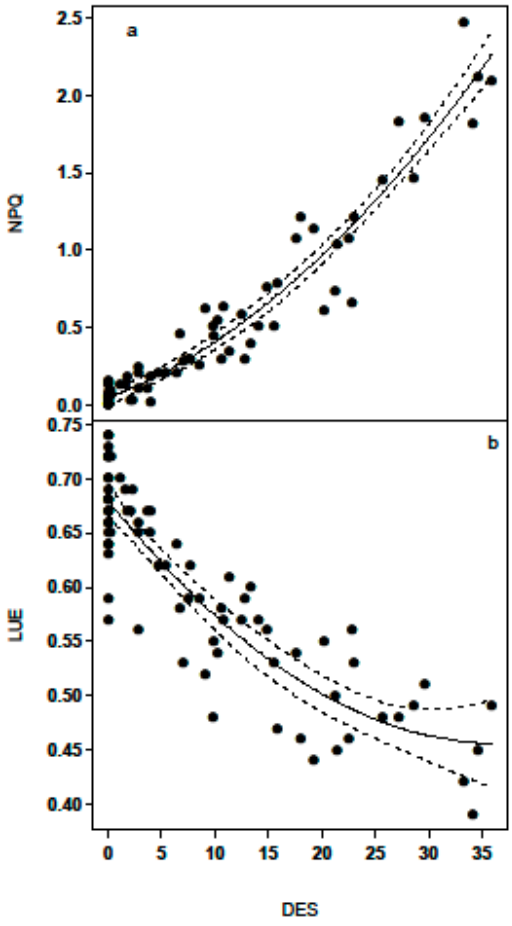

Figure 3. Relationships between NPQ and DES (a) and LUE and DES (b) without distinction of growth form and species. Equations of non-linear regressions are reported in the text (eq. 8 and 9). Dashed lines represent 95% IC.

Preprints (www.preprints.org) | NOT PEER-REVIEWED | Posted: 28 September 2016 doi:10.20944/preprints201609.0113.v1

3.3. Selection of relevant index from second derivative spectra

Spectral reflectance showed typical diatoms signatures [15,23] with specific pigment absorption bands respectively due to DD+DT (at 496 nm), Fuco (at 540 nm), Chl *c* (at 632 nm) and Chl *a* (at 588 and 673 nm) (Figure 4a). These absorption bands were confirmed using standardized (to Chl *c*) second derivatives spectra ($\delta\delta_{std}$, Figure 4b). However, DD+DT absorption band (around 496 nm) showed further absorption features (=shoulders) in 2nd derivative spectra, changing with light intensity as illustrated for *B. lucens* (Figure 5). Shoulders at 496, 500 and 505 nm were respectively assigned to DD+DT with a maximum during low light exposure (496 nm, DD+DT$_{LL}$), no change with light at 500 nm, and DD+DT$_{HL}$ increasing with light exposure (Figure 5). Shoulders at 487, 508 and 522 nm were assigned to xanthophyll absorptions features from literature: DD^{1} according to [25], DT^{3} according to [15] and the 'activated' DT (DT$^{4}_{NPQ}$), i.e. the molecules of DT effectively involved in NPQ [26,32] (Figure 5). Note that under our NSLC light conditions (i.e. 5 min exposure), DT arose from the xanthophyll cycle only (i.e. DD de-epoxidation) since no DT was synthesized '*de novo*' [33].

Preprints (www.preprints.org) | NOT PEER-REVIEWED | Posted: 28 September 2016 doi:10.20944/preprints201609.0113.v1

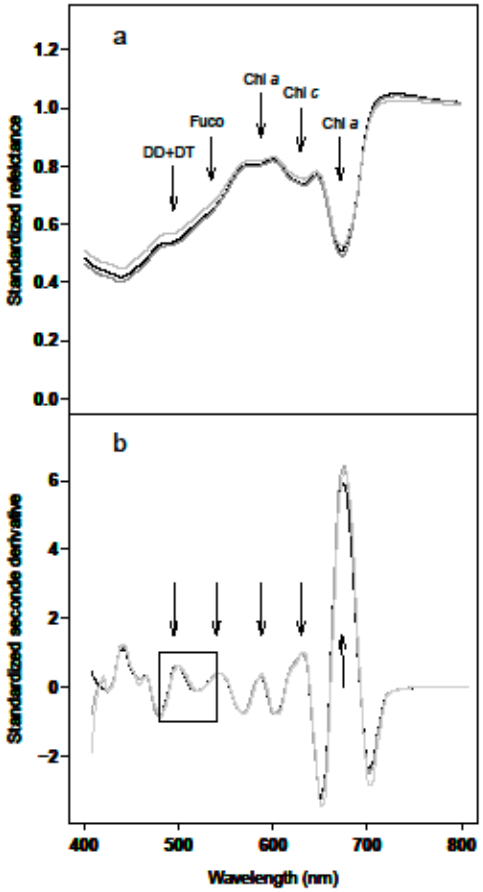

Figure 4. Characteristic radiometric spectra from a *B. lucens* culture exposed at three different light intensities (5 min): 0 (black line), 665 (grey line) and 1950 (clear grey line) µmol photons.m^{-2}.s^{-1}. a/ Standardized reflectance; b/ Standardized second derivative. Arrows show absorption bands at 496, 540, 588, 632 and 673 nm respectively due to DD+DT, Fuco, Chl *a*, Chl *c* and again Chl *a* (see text and [24]). The box delimits the absorption domain due to DD and DT xanthophylls (Figure 5).

Preprints (www.preprints.org) | NOT PEER-REVIEWED | Posted: 28 September 2016 doi:10.20944/preprints201609.0113.v1

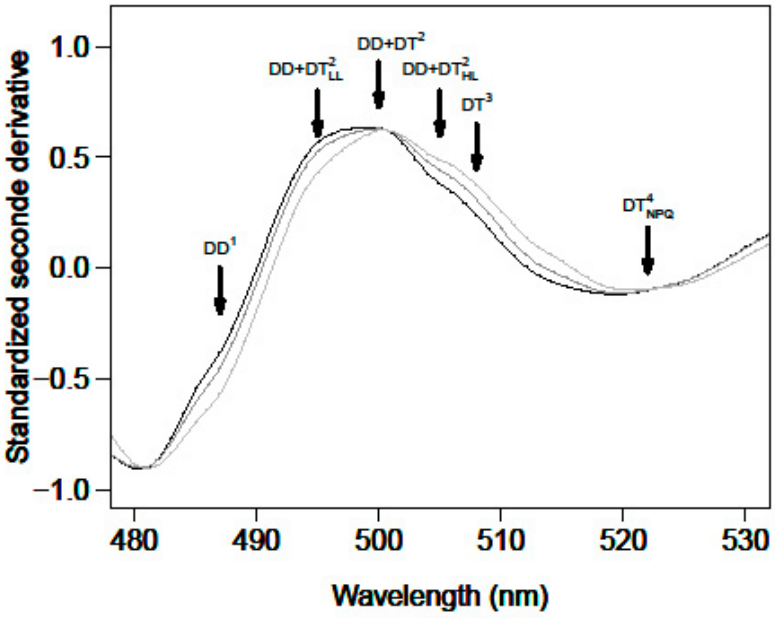

Figure 5. Zoom from Figure 4b for standardized second derivative over the absorption domain due to xanthophyll pigments involved in the XC (DD and DT) between 480 and 530 nm. Shoulders are assigned to absorption features of DD and DT from literature (DD^1, [25]; DT^3, [15]; and DT^4_{NPQ}, [26,32] and from this study ($DD+DT^2_{LL}$, $DD+DT^2$ and $DD+DT^2_{HL}$). For details see text.

These spectral features, were used to establish spectral indices build up as band ratios. Some indices were standardized to the Chl *c* absorption at 632 nm. Linear relationships were calculated between each index and LUE values measured by PAM-fluorometry for two growth forms: epipelic (represented by *N. phyllepta*) and epipsammic (represented by *B. lucens*). Thirteen indices displayed significant relationships (R^2> 0.4; $p \leq 0.05$; Table 2). Five fitted to both growth forms: $\delta\delta_{508/632}$; $\delta\delta_{496/505}$; $\delta\delta_{496/508}$; $\delta\delta_{500/505}$ and $\delta\delta_{500/508}$, seven fitted only to the epipsammic growth form: $\delta\delta_{496/632}$; $\delta\delta_{520/632}$; $\delta\delta_{496/500}$;

Preprints (www.preprints.org) | NOT PEER-REVIEWED | Posted: 28 September 2016 doi:10.20944/preprints201609.0113.v1

$\delta\delta_{496/520}$; $\delta\delta_{500/520}$; $\delta\delta_{505/520}$ and $\delta\delta_{508/520}$; one index, $\delta\delta_{505/632}$, fitted only to the epipelic growth form. Within these 13 linear regressions, only 6 indices (Table 2, in bold) allowed to predict LUE values of the three other species (*E. paludosa*, *P. delicatulum* and *P. vanheurckii*) with RSME values ≤ 0.02 (eq. 8 to 13):

$LUE = -3.130 \times \delta\delta_{505/632} + 1.702$ eq. 8

$LUE = 1.597 \times \delta\delta_{496/632} - 0.3466$ eq. 9

$LUE = -5.313 \times \delta\delta_{520/632} + 0.027$ eq. 10

$LUE = 0.056 \times \delta\delta_{496/508L} + 0.247$ eq. 11

$LUE = 0.064 \times \delta\delta_{496/508S} + 0.258$ eq. 12

$LUE = 0.190 \times \delta\delta_{500/520} + 1.316$ eq. 13

Most of these six indices were species specific (Table 2), except $\delta\delta_{496/508}$ which could be used for both *N. phyllepta* and *B. lucens* (Table 2, equations 11 and 12). Analyses of covariance were performed with all the six regressions and confirmed that only those involving $\delta\delta_{496/508L}$ and $\delta\delta_{496/508S}$ were not significantly different (ANCOVA, $p>0.05$), and therefore not be affected by species. For this reason, we propose a single relationship based on the index $\delta\delta_{496/508}$ to predict LUE for all species and corresponding growth forms:

$LUE = 0.049 \times \delta\delta_{496/508} + 0.317$ eq. 14

Since this index was not affected by species, it was selected for ETR prediction and hereafter called the MPB_{LUE} index.

Preprints (www.preprints.org) | NOT PEER-REVIEWED | Posted: 28 September 2016 doi:10.20944/preprints201609.0113.v1

Table 2. Spectral indices explaining more than 40 % of the variability (R^2 > 0.4) of the LUE estimated by PAM-fluorometry using *Navicula phyllepta* and *Biremis lucens* data set. The lowest values of RSME (=Root Mean Square Error), in bold, to predict LUE for *Entomoneis paludosa*, *Planothidium delicatulum* and *Plagiogrammopsis vanheurckii* are those selected (eq. 8 to 13). n.t.: no tested.

Table 2a. Indices calculated using second derivative value standardized to the Chl *c* red band absorption.

Table 2b. Indexes calculated using only pigments involved in xanthophyll cycle.

	R^2		RSME		
	N. phyllepta	*B. lucens*	*E. paludosa*	*P. delicatulum*	*P. vanheurckii*
Table 2a					
$\delta\delta_{496/632}$	< 0.4	**0.49*****	n.t	**0.01**	0.28
$\delta\delta_{505/632}$	**0.51****	< 0.4	**0.01**	n.t	0.03
$\delta\delta_{508/632}$	0.61***	0.73***	0.05	0.12	n.t
$\delta\delta_{520/632}$	< 0.4	**0.61*****	n.t	**0.01**	0.11

Preprints (www.preprints.org) | NOT PEER-REVIEWED | Posted: 28 September 2016 doi:10.20944/preprints201609.0113.v1

Table 2b					
$\delta\delta_{496/500}$	< 0.4	0.61***	n.t	0.05	n.t
$\delta\delta_{496/505}$	0.42**	0.74***	0.14	0.11	n.t
$\delta\delta_{496/508}$	**0.47****	**0.71*****	0.13	**0.00**	**0.01**
$\delta\delta_{496/520}$	< 0.4	0.40***	n.t	0.3	n.t
$\delta\delta_{500/505}$	0.42**	0.76***	0.11	0.12	n.t
$\delta\delta_{500/508}$	0.44**	0.85***	0.09	0.26	n.t
$\delta\delta_{500/520}$	< 0.4	**0.72*****	n.t	**0.02**	0.15
$\delta\delta_{505/520}$	< 0.4	0.85***	n.t	0.04	n.t
$\delta\delta_{508/520}$	< 0.4	0.90***	n.t	0.06	n.t

Preprints (www.preprints.org) | NOT PEER-REVIEWED | Posted: 28 September 2016 doi:10.20944/preprints201609.0113.v1

3.4. Electron transfer rate prediction using MPB_{LUE} index.

ETR prediction following eq. 3 and 4, needed the estimation of LUE by radiometry (from eq.14), but also the optical absorption cross-section (a*) retrieved from the radiative transfer model MPBOM applied to each reflectance spectrum. We verified that the a* parameter remained stable at all light levels for all diatom species with a mean value of 0.09 m^2.mg Chla^{-1} ± 0.01 SD (ANOVA, p=0.9, Figure 6). ETR predictions based on the MPB_{LUE} index showed a highly significant linear relationship with measured PAM-fluorometry ETR (R^2 = 0.92, p<0.001; Figure 7) with a slope of 0.93 not significantly different from 1 (p>0.05).

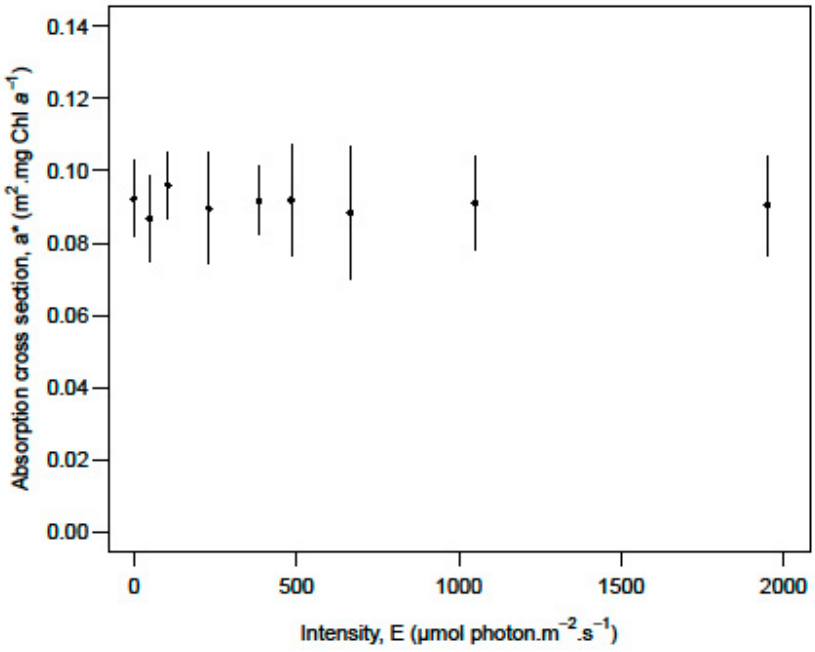

Figure 6. Optical absorption cross-section a* as retrieved from the MPBOM transfer radiative model [22] and averaged over the Chl *a* absorption domain (670 to 685 nm) and for all species. Vertical bars represent standard deviation.

Preprints (www.preprints.org) | NOT PEER-REVIEWED | Posted: 28 September 2016 doi:10.20944/preprints201609.0113.v1

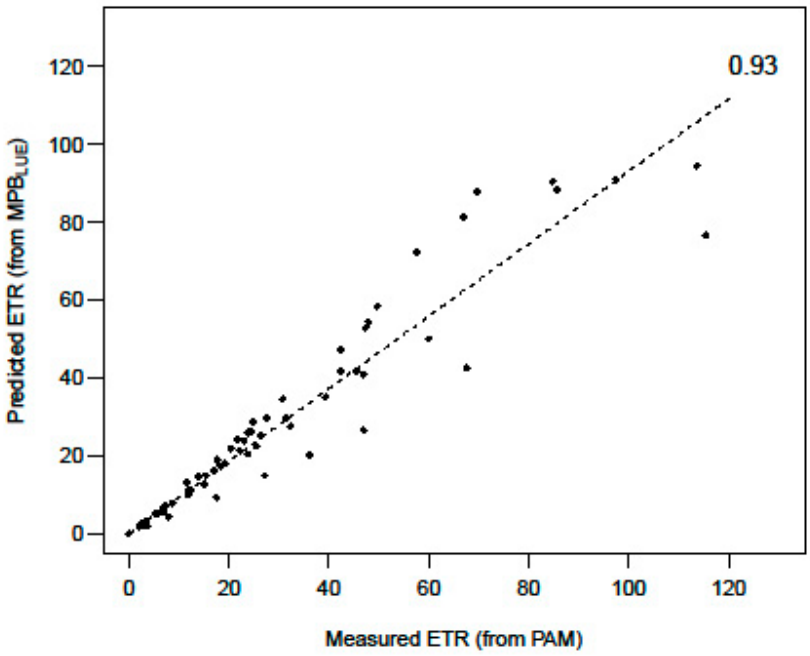

Figure 7. Measured ETR (from PAM fluorometry) *vs*. predicted ETR (from radiometric measurements using the MPB_{LUE} index). The dash line is the slope (=0.93) of the linear regression (R^2 = 0.92, $p<0.001$). All species and growth forms were included.

4. Discussion

4.1. Selection of a radiometric index for ETR prediction: the MPB_{LUE} index.

The objective of this study was to find a radiometric index to predict ETR from reflectance spectra as a proxy for MPB primary production. The choice of PAM-fluorometry to estimate ETR to calibrate a radiometric index was based on the fact that data time acquisition is in the same time range for both techniques. Using NSLCs and other light curves [16], photosynthetic parameters and reflectance data are obtained in less than 1 second [34] reflecting similar involved processes. Alternative techniques [16] require much longer measuring times, e.g. CO_2 fluxes using benthic chambers or O_2

Preprints (www.preprints.org) | NOT PEER-REVIEWED | Posted: 28 September 2016 doi:10.20944/preprints201609.0113.v1

fluxes using micro-electrodes can take more than 20 min [35]; ^{14}C based techniques take even longer [36], due to processes more longer than pigment de-epoxydation or electron transfer. Furthermore, radiometric data are closely linked to pigment composition as any change in pigment content is known to induce reflectance and second derivative spectral changes [24,37]. Changes in chlorophyll fluorescence (especially via NPQ) is also closely related to pigment composition, namely to the xanthophylls DD and DT [15,38–40]. For these two reasons, i.e. time scale and strong relationship to pigments, PAM-fluorometry is probably the most robust technique to be coupled with spectroradiometry.

From all the relationships tested in this study, one index was selected, i.e. the MPB_{LUE} index ($\delta\delta_{496/508}$) because it was independent of species and growth forms. This is an unexpected result because diatom growth forms strongly affect eco-physiological response to light exposure as demonstrated previously by [17]. It was confirmed by the present work with expected differences between epipsammon and epipelon de-epoxydation responses (i.e. highest and lowest, respectively, see [17]). Although DES differences were significant between growth forms, it did not affect ETR prediction using the MPB_{LUE} index. This is ideal for remote sensing applications since the MPB_{LUE} index could be applied to natural microphytobenthic assemblages independently of their growth form/specific composition.

All indices investigated here were mainly linked to DD and/or DT absorption bands around 500 nm. Globally, absorption before 500 nm decreased with light whereas over 500 nm it increased. This pattern is due to the de-epoxydation of DD into DT as

Preprints (www.preprints.org) | NOT PEER-REVIEWED | Posted: 28 September 2016 doi:10.20944/preprints201609.0113.v1

previously reported by [15]. It explains why several indices identified in this study are close to the one proposed by [15], i.e. $\delta\delta_{508/632}$. However, the relationship between second derivative wavelength and LUE were not the same: [15] described an exponential relationship, whereas we found linear ones. This difference could be explained by: 1) light conditions (acclimation, intensity and duration) were different and responsible for range of LUE smaller in the current study; 2) Chl *c* content in species might have been different, leading to index variation not related to DES change but rather to a change in Chl *c* content due to species-dependent feature. This latter observation reinforces the use of the MPB_{LUE} index to predict ETR, because it is both species- and Chl *c*- independent.

The radiometric index based on the 522 nm absorption band was expected in this study to be more robust because this absorption has been shown to be a fingerprint for DT molecules effective in NPQ [26,32]. However, among the species used here, only *B. lucens* showed a strong relationship between PAM and radiometric indices using 522 nm band. The weakness of 522 nm-based indices in *N. phyllepta* data was likely due to the low DES and DT content, and the subsequent low NPQ [17]. DT content might be too low to be detected by radiometry, a less sensitive method than the spectrophotometric approaches used before [26,32].

4.2. Remote sensing applications

Remote sensing has been used to map MPB biomass, using multi- and hyperspectral imager [7,9–12,41]. More recently, it was used to estimate optical absorption cross section (=a*) retrieved from optical properties of the MPB biofilm [22,24]. The current

Preprints (www.preprints.org) | NOT PEER-REVIEWED | Posted: 28 September 2016 doi:10.20944/preprints201609.0113.v1

study is a step further in VIS-NIR remote sensing to potentially map MPB primary production.

Although the present study calls for promising applications, before being able to estimate ETR at the ecosystem level using the MPB_{LUE} index some challenges still need to be addressed, particularly with the spatial and the temporal up-scaling. It is well known that MPB shows a patchy biofilm distribution at both the micro- and the macro-scales [42] leading to non-linear mixing of the biomass [9,43] at the pixel scale. This constraints remote sensing applications, because using linear model as indices (e.g. NDVI, MPBI, I_{diatom}, see [10] and the index MPB_{LUE}) and/or radiative transfer models (e.g. MPBOM) could lead to misestimating biomass, LUE, and thus ETR when distribution of biofilm is too patchy. The best way to limit this misestimation is to work at very high spatial resolution (m^2 and less), and at a very high spectral resolution (at least ~100 spectral bands). Consequently, MPB_{LUE} application in MPB primary production models will require the utilization of hyperspectral images coupling high spectral and spatial resolutions. Hyperspectral images with high spatial resolution are currently acquired from airborne campaign, but not yet from spatial satellite, even if some projects are planned, i.e. the CNES (French Spatial Agency) project HYPXIM or the DLR (German Spatial Agency) project EnMap.

Another expected difficulty is the species composition of the natural assemblages. It should be possible to roughly separate epipsammic and epipelic assemblages by mapping grain-size of sediment constituting mudflat using hyperspectral images [44]. Mixed sediments could be considered as inhabited by epipsammic assemblages, whereas muddy sediment by epipelic ones [45–47]. However, each assemblage can host other growth forms: e.g. epipelic growth forms in epipsammic assemblage or

Preprints (www.preprints.org) | NOT PEER-REVIEWED | Posted: 28 September 2016 doi:10.20944/preprints201609.0113.v1

thycoplanktonic growth forms in epipelic assemblage [48]. This could lead to a mix of photophysiological response of each growth form [17]. The present work shows that this limit can be overcome by the MPB_{LUE} index as it is only affected by the xanthophyll cycle: MPB_{LUE} index appears to have a wide-ranging property for growth form, as the NDVI for vegetation.

The temporal up-scaling issue is transversal to any MPB remote sensing approach and it is based on the drastic change of MPB biomass and specific composition during an emersion period [1,49,50]. In contrast, reflectance images are acquired instantaneously and the derived ETR maps would thus assess primary production at a single acquisition time which would inevitably induce a strong bias for tidal scale as well as daily budget estimation. Such problem could be overcome by performing several flights over the mudflat through the same pathway coupled to interpolation model to fill gaps between images. With spatial sensors, this approach could be achieved only with a geostationary platform.

5. Concluding remarks

Hyperspectral remote sensing is a highly promising technology to achieve MPB ETR and subsequent primary production estimation at the ecosystem level. Here we showed how a new robust index, the MPB_{LUE} based on reflectance data in the DD and DT absorption domain, can be used to estimate ETR from hyperspectral imagery. Nevertheless, several constraints related to MPB temporal and spatial variability remains to be overcome. We demonstrated that the species diversity analyzed in this study did not affect MPB_{LUE} index, and it can be applied to epipelic, epipsammic and thycoplankton species in mixture, i.e. in mixed sediments. It will be especially useful for

the scarcely studied MPB assemblages dominated by epipsammon in sandy flats. MPB spatial and temporal variability at meso-scale (several m^2 and min) could be mapped using high spatial resolution and high image acquisition frequency which will possible with new satellite sensors in the years to come. Meanwhile, further work is needed to thoroughly determine the relationship between reflectance, ETR and Carbone fixation in order to build maps of Carbone fluxes (mg $CO_2.h^{-1}.m^{-2}$, [51]) at the scale of entire mudflats.

6. Acknowledgments

The authors acknowledge the Centre National de la Recherche Scientifique-CNRS and the Region Poitou-Charentes, for their financial support; the Planetology and Geodynamic laboratory (UMR 6112, University of Nantes-CNRS) for ASD FieldSpec3spectrometer supply.

7. Author Contributions

All authors has substantially contributed to the design of the study, the production, analysis, or interpretation of the results, and/or preparation of the manuscript

8. Conflicts of Interest

The authors declare no conflict of interest.

9. References

1. Consalvey, M.; Paterson, D. M.; Underwood, G. J. C. The ups and downs of life in a benthic biofilm: Migration of benthic diatoms. *Diatom Res.* **2004**, *19*, 181–202.

2. MacIntyre, H.; Geider, R.; Miller, D. Microphytobenthos: the ecological role of the "secret garden" of unvegetated, shallow water marine habitats. I. Distribution, abundance and primary production. *Estuaries.* **1996**, *19*, 186–201.

3. Pinckney, J.; Zingmark, R. G. Biomass and Production of Benthic Microalgal Communities in Estuarine Habitats. *Estuaries* **1993**, *16*, 887–897.

4. Underwood, G. J. C.; Kromkamp, J. Primary production by phytoplancton and microphytobenthos in estuaries. *Adv Ecol Res* **1999**, *29*, 93–153.

5. Kromkamp, J.; Forster, R. M. Development in microphytobenthos primary productivity studies. In *Functioning of microphytobenthos in estuaries*; Kromkamp, J.; de Brouwer, J. F. C.; Blanchard, G. F.; Forster, R. M.; Creach, V., Eds.; Edita, 2006; pp. 9–30.

6. Guarini, J. M.; Blanchard, G.; Richard, P. Modelling the dynamics of the microphytobenthic biomass and primary production in European intertidal mudflats. In *Functioning of microphytobenthos in estuaries*; Kromkamp, J.; de Brouwer, J. F. C.; Blanchard, G. F.; Forster, R. M.; Creach, V., Eds.; Edita, 2006; pp. 187–226.

7. Benyoucef, I.; Blandin, E.; Lerouxel, A.; Jesus, B.; Rosa, P.; Meleder, V.; Launeau, P.; Barille, L. Microphytobenthos interannual variations in a north-European estuary (Loire estuary, France) detected by visible-infrared multispectral remote sensing. *Estuar. Coast. Shelf Sci.* **2014**, *136*, 43–52.

8. Brito, A. C.; Benyoucef, I.; Jesus, B.; Brotas, V.; Gernez, P.; Mendes, C. R.; Launeau, P.; Dias, M. P.; Barille, L. Seasonality of microphytobenthos revealed by remote-sensing in a South European estuary. *Cont. Shelf Res.* **2013**, *66*, 83–91.

9. Combe, J. P.; Launeau, P.; Carrere, V.; Despan, D.; Meleder, V.; Barille, L.; Sotin, C. Mapping microphytobenthos biomass by non-linear inversion of visible-infrared hyperspectral images 10.1016/j.rse.2005.07.010. *Remote Sens. Environ.* **2005**, *98*, 371–387.

10. Kazemipour, F.; Launeau, P.; Méléder, V. Microphytobenthos biomass mapping using the optical model of diatom biofilms: Application to hyperspectral images of Bourgneuf Bay. *Remote Sens. Environ.* **2012**, *127*, 1–13.

11. Ryu, J.-H.; Choi, J.-K.; Lee, Y.-K. Potential of remote sensing in management of tidal flats: A case study of thematic mapping in the Korean tidal flats. *Ocean Coast. Manag.* **2014**, *102*, 458–470.

12. van der Wal, D.; Wielemaker-van den Dool, A.; Herman, P. M. Spatial synchrony in intertidal benthic algal biomass in temperate coastal and estuarine ecosystems. *Ecosystems* **2010**, *13*, 338–351.

13. Huete, A.; Ponce-Campos, G.; Zhang, Y.; Restrepo-Coupe, N.; Ma, X.; Moran, M. S. Monitoring Photosynthesis From Space. In *Land Resources Monitoring, Modeling, and Mapping with Remote Sensing*; Thenkabail, P. S., Ed.; CRC Press, 2015; Vol. II, pp. 3–22.

14. Consalvey, M.; Perkins, R. G.; Paterson, D. M. PAM fluorescence: a beginners guide for benthic diatomists. *Diatom Res.* **2005**, *20*, 1–22.

15. Jesus, B.; Mouget, J.-L.; Perkins, R. G. Detection of diatom xanthophyll cycle using spectral reflectance. *J. Phycol.* **2008**, *44*, 1349–1359.

16. Perkins, R.; Kromkamp, J. C.; Serodio, J.; Lavaud, J.; Jesus, B.; Mouget, J. L.; Lefebvre, S.; Forster, R. M. The application of variable chlorophyll fluorescence to microphytobenthic

biofilms. In *Use of Chlorophyll Fluorescence in Aquatic Sciences*; Prasil, O.; Sugget, D., Eds.; Developments in Aplied Phycology; 2011; Vol. 4.

17. Barnett, A.; Méléder, V.; Blommaert, L.; Lepetit, B.; Gaudin, P.; Vyverman, W.; Sabbe, K.; Dupuy, C.; Lavaud, J. Growth form defines physiological photoprotective capacity in intertidal benthic diatoms. *Isme J.* **2015**, *9*, 32–45.

18. Juneau, P.; Barnett, A.; Méléder, V.; Dupuy, C.; Lavaud, J. Combined effect of high light and high salinity on the regulation of photosynthesis in three diatom species belonging to the main growth forms of intertidal flat inhabiting microphytobenthos. *J. Exp. Mar. Biol. Ecol.* **2015**, *463*, 95–104.

19. Guillard, R. R. L. Culture of phytoplankton for feeding marine invertebrates. In *Culture of marine invertebrate animals*; Smith, W. L.; Chanly, M. H., Eds.; Plenum Press: New York, 1982; pp. 108–132.

20. Lavaud, J.; Rousseau, B.; Etienne, A. L. General features of photoprotection by energy dissipation in planktonic diatoms (Bacillariophyceae). *J. Phycol.* **2004**, *40*, 130–137.

21. Perkins, R. G.; Mouget, J. L.; Lefebvre, S.; Lavaud, J. Light response curve methodology and possible implications in the application of chlorophyll fluorescence to benthic diatoms 10.1007/s00227-005-0222-z. *Mar. Biol.* **2006**, *149*, 703–712.

22. Kazemipour, F.; Meleder, V.; Launeau, P. Optical properties of microphytobenthic biofilms (MPBOM): Biomass retrieval implication. *J. Quant. Spectrosc. Radiat. Transf.* **2011**, *112*, 131–142.

23. Meleder, V.; Barille, L.; Launeau, P.; Carrere, V.; Rince, Y. Spectrometric constraint in analysis of benthic diatom biomass using monospecific cultures 10.1016/j.rse.2003.08.009. *Remote Sens. Environ.* **2003**, *88*, 386–400.

24. Meleder, V.; Laviale, M.; Jesus, B.; Mouget, J.-L.; Lavaud, J.; Kazemipour, F.; Launeau, P.; Barille, L. In vivo estimation of pigment composition and optical absorption cross-section by spectroradiometry in four aquatic photosynthetic micro-organisms. *J. Photochem. Photobiol. B-Biol.* **2013**, *129*, 115–124.

25. Olaizola, M.; Yamamoto, H. Short-term response of the diadinoxanthin cycle and fluorescence yield to high irradiance in diatoms (Bacillariophyceue). *J Phycol* **1994**, *30*, 606–612.

26. Ruban, A. V.; Lavaud, J.; Rousseau, B.; Guglielmi, G.; Horton, P.; Etienne, A. L. The super-excess energy dissipation in diatom algae: comparative analysis with higher plants. *Photosynth. Res.* **2004**, *82*, 165–175.

27. Wilhelm, C. The biochemistry and physiology of light-harvesting process in chlorophyll b and chlorophyll c-containing algae. *Plant Physiol Biochem* **1990**, *28*, 293–306.

28. Falkowski, P. G.; Raven, J. A. *Aquatic Photosynthesis - Second Edition*; Princeton University Press: Princeton, 2007.

29. Parson, W. W.; Nagarajan, V. Optical Spectroscopy in Photosynthetic Antennas. In *Light-Harvesting Antennas in Photosynthesis*; Green, B. R.; Parson, W. W., Eds.; Advances in Photosynthesis and Respiration; Kluwer Academic Publishers: Dordrecht, 2003; pp. 83–127.

30. Roy, S.; Llewellyn, C.; Egeland, E. S.; Johnsen, G. *Phytoplankton Pigments - Characterization, Chemotaxonomy and Applications in Oceanography*; SCOR, Ed.; Cambridge University Press: Cambridge, 2011.

31. Serodio, J.; Lavaud, J. A model for describing the light response of the nonphotochemical quenching of chlorophyll fluorescence. *Photosynth. Res.* **2011**, *108*, 61–76.

32. Lavaud, J.; Lepetit, B. An explanation for the inter-species variability of the photoprotective non-photochemical chlorophyll fluorescence quenching in diatoms. *Biochim. Biophys. Acta BBA - Bioenerg.* **2013**, *1827*, 294–302.

33. Lavaud, J.; Goss, R. The peculiar features of non-photochemical fluorescence quenching in diatoms and brown algae. In *Non-Photochemical Quenching and Energy Dissipation in Plants, Algae and Cyanobacteria*; Springer, 2014; pp. 421–443.

34. Serodio, J. A chlorophyll fluorescence index to estimate short-term rates of photosynthesis by intertidal microphytobenthos. *J. Phycol.* **2003**, *39*, 33–46.

35. Migne, A.; Davoult, D.; Spilmont, N.; Menu, D.; Boucher, G.; Gattuso, J. P.; Rybarczyk, H. A closed-chamber CO2-flux method for estimating intertidal primary production and respiration under emersed conditions. *Mar. Biol.* **2002**, *140*, 865–869.

36. Blanchard, G.; Guarini, J.-M.; Gros, P.; Richard, P. Seasonal effect on the relationship between the photosynthetic capacity of intertidal microphytobenthos and temperature. *J. Phycol.* **1997**, *3*, 723–728.

37. Jesus, B.; Rosa, P.; Mouget, J.-L.; Meleder, V.; Launeau, P.; Barille, L. Spectral-radiometric analysis of taxonomically mixed microphytobenthic biofilms. *Remote Sens. Environ.* **2014**, *140*, 196–205.

38. Goss, R.; Jakob, T. Regulation and function of xanthophyll cycle-dependent photoprotection in algae. *Photosynth. Res.* **2010**, *106*, 103–122.

39. Lavaud, J. Fast regulation of photosynthesis in diatoms : Evolution, regulation and ecophysiology. *Funct. Plant Sci. Biotechnol.* **2007**, *1*, 267–387.

40. Lohr, M.; Wilhelm, C. Pigment synthesis and xanthophyll cycle in diatoms under high light stress and during low light recovery. In *Photosynthesis: Mechanisms and effets*; Garab, G., Ed.; Kluwer Academic Publishers: Dordrecht, The Netherlands, 1998; pp. 2313–2316.

41. Meleder, V.; Launeau, P.; Barillé, L.; Rincé, Y. Microphytobenthos assemblage mapping by spatial visible-infrared remote sensing in a shellfish ecosystem 10.1016/s1631-0691(03)00125-2. *C. R. Biol.* **2003**, *326*, 377–389.

42. Saburova, M. A.; Polikarpov, I. G.; Burkovsky, I. V. Spatial structure of an intertidal sandflat microphytobenthic community as related to different spatial scales. *Mar Ecol Prog Ser* **1995**, *129*, 229–239.

43. Meleder, V.; Launeau, P.; Barille, L.; Combe, J. P.; Carrere, V.; Jesus, B.; Verpoorter, C. Hyperspectral imaging for mapping microphytobenthos in coastal areas. In *Geomatic solutions for coastal environments*; Maanan, M.; Robin, M., Eds.; Nova Science Publishers, Inc., 2010; pp. 71–139.

44. Verpoorter, C.; Carrère, V.; Combe, J.-P. Visible, near-infrared spectrometry for simultaneous assessment of geophysical sediment properties (water and grain size) using the Spectral Derivative–Modified Gaussian Model. *J. Geophys. Res. Earth Surf.* **2014**, *119*, 2098–2122.

45. Hamels, I.; Sabbe, K.; Muyleart, K.; Barranguet, C.; Lucas, C.; Herman, P.; Vyverman, W. Organisation of microbenthic communities in intertidal estuarine flats, a case study from the Molenplaat (Westerschelde estuary, The Netherlands). *Eur. J Protistol* **1998**, *34*, 308–320.

46. Meleder, V.; Rincé, Y.; Barillé, L.; Gaudin, P.; Rosa, P. Spatiotemporal changes in microphytobenthos assemblages in a macrotidal flat (Bourgneuf Bay,France). *J. Phycol.* **2007**, *43*, 1177–1190.

47. Paterson, D. M.; Hagerthey, S. E. Microphytobenhthos in contrasting coastal ecosytems: Biology and Dynamics. In *Ecological Comparisons of Sedimentary Shores*; Reise, K., Ed.; Spring-Verlag: Berlin Heidelberg, 2001; Vol. 151, pp. 105–125.

48. Ribeiro, L.; Brotas, V.; Mascarell, G.; Coute, A. Taxonomic survey of the microphytobenthic communities of two Tagus estuary mudflats. *Acta Oecologica* **2003**, *24*, S117–S123.

49. Jesus, B.; Brotas, V.; Ribeiro, L.; Mendes, C. R.; Cartaxana, P.; Paterson, D. M. Adaptations of microphytobenthos assemblages to sediment type and tidal position. *Cont. Shelf Res.* **2009**, *29*, 1624–1634.

50. Serodio, J.; Silva, J. M. d.; Catarino, F. Nondestructive tracing of migratory rhythms of intertidal benthic microalgae in vivo chlorophyll a fluorescence. *J. Phycol.* **1997**, *33*, 542–553.

51. Morris, E. P.; Forster, R. M.; Peene, J.; Kromkamp, J. C. Coupling between Photosystem II electron transport and carbon fixation in microphytobenthos. *Aquat. Microb. Ecol.* **2008**, *50*, 301–311.

Legend of Figures

Figure 1. Specimens of the five diatom species viewed in scanning electron microscopy. Scale bars represent 1 µm. Credits Nantes Culture Collection (NCC). *Navicula phyllepta* and *Entomoneis paludosa* belong to the epipelic growth form; *Biremis lucens* and *Planothidium delicatulum* belong to the epipsammic one; *Plagiogrammopsis vanheurckii* is thycoplanktonic.

Figure 2. DES *versus* light intensity after 5 min exposure for the three growth forms: ●Epipelic (*Navicula phyllepta* and *Entomoneis paludosa*); ■Epipsammic (*Biremis lucens* and *Planothidium delicatulum*); ◆Thycoplanktonic (*Plagiogrammopsis vanheurckii*). Averaged DES were fitted using the model proposed by [31], vertical bars represent standard deviation.

Figure 3. Relationships between NPQ and DES (a) and LUE and DES (b) without distinction of growth form and species. Equations of non-linear regressions are reported in the text (eq. 8 and 9). Dashed lines represent 95% IC.

Figure 4. Characteristic radiometric spectra from a *B. lucens* culture exposed at three different light intensities (5 min): 0 (black line), 665 (grey line) and 1950 (clear grey line) µmol photons.m^{-2}.s^{-1}. a/ Standardized reflectance; b/ Standardized second derivative. Arrows show absorption bands at 496, 540, 588, 632 and 673 nm respectively due to DD+DT, Fuco, Chl *a*, Chl *c* and again Chl *a* (see text and [24]). The box delimits the absorption domain due to DD and DT xanthophylls (Figure 5).

Preprints (www.preprints.org) | NOT PEER-REVIEWED | Posted: 28 September 2016 doi:10.20944/preprints201609.0113.v1

Figure 5. Zoom from Figure 4b for standardized second derivative over the absorption domain due to xanthophyll pigments involved in the XC (DD and DT) between 480 and 530 nm. Shoulders are assigned to absorption features of DD and DT from literature (DD^{1}, [25]; DT^{3}, [15]; and DT^{4}_{NPQ}, [26,32] and from this study ($DD+DT^{2}_{LL}$, $DD+DT^{2}$ and $DD+DT^{2}_{HL}$). For details see text.

Figure 6. Optical absorption cross-section a* as retrieved from the MPBOM transfer radiative model [22] and averaged over the Chl *a* absorption domain (670 to 685 nm) and for all species. Vertical bars represent standard deviation.

Figure 7. Measured ETR (from PAM fluorometry) *vs*. predicted ETR (from radiometric measurements using the MPB_{LUE} index). The dash line is the slope (=0.93) of the linear regression ($R^2 = 0.92$, $p<0.001$). All species and growth forms were included.

Figure S1. Standardized (to 500 nm) second derivative spectra from pre-experimentation using *N. phyllpeta* culture, after 5 min in the dark obtained on two different backgrounds: black (black line) and white (grey line). With black background, the xanthophyll cycle was not activated, contrary to white one. Activation of the xanthophyll cycle was shown by the increase of second derivatives values after 500 nm (see Figure 5).